Journal of Ceramic Processing Research. Vol. 25, No. 4, pp. 483~489 (2024)
(Received 12 September 2023, Received in revised form 29 November 2023, Accepted 4 December 2023)
https://doi.org/10.36410/jcpr.2024.25.4.483

J O U R N A L O F
Ceramic Processing Research

Mechanical properties of silicon carbide/graphene nanoplatelets composites prepared by spark plasma sintering

Zhang Xiuling[a], Chen Yuhong[a,b,*], Liu Limeng[a], Qi Wubin[a], Hai Wanxiu[a,b], Xue Min[a] and Hong Tianxiang[a]
[a]*School of Materials Science and Engineering, North Minzu University, Yinchuan, 750021, China*
[b]*Key Lab of Powder Material & Advanced Ceramics, Yinchuan 750021, China*

Silicon carbide (SiC)/graphene nanoplatelets (GNPs) ceramic composites with additions of 0, 1, 2, 4, 6, 8 wt.% GNPs were fabricated by spark plasma sintering (SPS). Effects of GNPs addition on densification, microstructure and mechanical properties (vickers hardness and fracture toughness) of the SiC/GNPs composites were investigated. As GNPs content increased, relative density of the composites decreased slightly from 99.0% for monolithic SiC to 98.3% at 8 wt.% GPNs. Uniform distribution of GNPs in the microstructure was exhibited. Vickers hardness was increased by 7% (25.4 GPa) in the 1 wt.% GNPs composition relative to monolithic SiC (23.5 GPa). The Vickers hardness and fracture toughness changes indicated different states of GNPs existence in the SiC/GNPs composites, among which thin-layered GNPs wrapping SiC grains could benefit Vickers hardness relative to agglomeration of GNPs.

Keywords: Silicon carbide, Graphene nanoplatelets, Microstructure, Mechanical properties.

Introduction

Mechanical properties improvement is always crucial for structural ceramics for applications in conditions where high hardness, fracture toughness and strength are required. SiC as one of the most widely used structural ceramics faces the same situation, though SiC ceramics usually show relatively good flexural strength and hardness reaching 800 MPa and 20 GPa, respectively [1-3]. In the last few years, graphene-based nanostructures have attracted extensive research as a good reinforcement to ceramics due to high tensile strength and Young's modulus reaching 130 GPa and 0.5-1 TPa of thin-layered GNPs [4-6]. In liquid phase-sintered SiC ceramics, introduction of rGO (reduced graphene oxide) or GNPs sheets seems to reduce local stresses/strains at crack tips to inhibit crack propagation, hence higher toughness [7-9]. Manuel Belmonte et al. [10] observed a fracture toughness value as high as 8.3 MPa·m$^{1/2}$ for a liquid phase sintering SiC ceramic prepared by SPS and using 5% rGO as the reinforcing additive. This fracture toughness value was increased about by ~162% relative to monolithic SiC. Miranzo et al. [11] also prepared SiC/graphene composites by SPS and demonstrated a similar increase in fracture toughness (by ~55%) when graphene sheets (about 4 vol%) grew in-situ in the SiC ceramics.

Contrary to liquid phase-sintered SiC ceramics, reinforcing effects of GNPs in solid state sintered SiC is relatively weak, and simultaneously, reason for the less significant reinforcing effects is not clear yet. The solid state-sintered SiC ceramics usually use boron, carbon or boron carbide as sintering additives. Li et al. [12] prepared solid state-sintered SiC with graphene content increasing from 0 to 5.0 wt.%. Fracture toughness of the 1.0 wt.% graphene composition (5.65 MPa·m$^{1/2}$) was only 22% higher than that for monolithic SiC. Bódis et al. [13] prepared SiC by SPS using boron powder as solo sintering aid. Again, the SiC ceramic with 3 wt.% graphene addition exhibited a maximum increase in Vickers hardness and fracture toughness by 17% and 22%, respectively, relative to that for monolithic SiC. On the other hand, it has also been reported that the addition of GNPs inhibits the densification of ceramics and reduces Vickers hardness. Kaźmierczak-Bałata [14] prepared SiC with co-additions of boron and carbon by SPS and reported decrease in density and fracture toughness when GNPs was added. Guo [15] prepared SiC/GNPs composites by pressureless sintering using B_4C as sintering additive. Similarly, bending strength and hardness of the SiC/GNPs composites decreased decreased by 50.0% and 37.7%, respectively when added to 10 wt.% GNPs. Different thermal expansion coefficients of GNP$_S$ from SiC were thought as a reason for mechanical property decrease. But it is believed that the reason should not be so simple.

Herein, solid state sintered SiC ceramics using 0.8 wt.% B_4C in combination with 2 wt.% carbide as the sintering aid were prepared by SPS. Effects of GNPs addition (0, 1, 2, 4, 6, and 8 wt.% GNPs) on microstructure and mechanical properties of the SiC

*Corresponding author:
Tel : 13079598519
Fax: 0086-951-2066827
E-mail: lyhchen@163.com

ceramics were investigated. The results revealed that fracture toughness of the SiC/GNPs composites could be increased if GNP_S was dispersed sufficiently, while hardness and elastic modulus may be traded off in some extent, depending on the GNPs content.

Experimental

Materials

α-SiC powers (H.C. Stack, Germany), GNPs (HeFei Vihon Materials Technology, China), B_4C (Macklin, China) and glucose (Aladdin, China) were used as raw materials. The SiC powder had an average particle size of 0.6 μm. The GNPs was about 3 nm in thickness, with an average specific surface area around 150 $m^2 \cdot g^{-1}$. Glucose was used as the carbon source.

SiC, B_4C and glucose slurries were prepared by SiC ball milling on rolles in plastic jar with SiC balls for 8 h in DI water. GNPs were dispersed in DI water at 40°C for 6 h with an ultrasonic probe at a power of 240 W by ultrasonic method. Thereafter, 1, 2, 4, 6, 8 wt.% GNPs solution was distilled into the SiC, B_4C and glucose slurries while the slurries were homogenized by magnetic-ultrasonic stirring. Complete addition of a GNPs solution to a SiC slurry usually took about 4 h. After further homogenizing for 4 h, the mixture was dried in open air at 100°C and sieved for sintering.

The powder mixtures were calcined in a graphite resistance furnace (SKY, Norbert measurement and control technology Ltd. China) at 1200°C for 90 min to convert the glucose content into carbon. The densification was performed in Ar atmosphere at 2000°C or 2050°C for 10 min under uniaxial pressure of 25 MPa in SPS (SPS-20T-10, Chen Hua Technology Company Limited, China).

At first stage of sintering (from RT to 1400°C) heating rate of 20°C/min was used, then to reach final temperature, heating rate of 10°C/min was used. Dimensions of prepared samples were 25 mm in diameter and thickness approximately 4 mm.

Characterization

Bulk density was measured by the Archimedes principle. Theoretical density was determined by the law of mixtures taking density of SiC and GNPs as 3.2 $g \cdot cm^{-3}$ and 2.2 $g \cdot cm^{-3}$, respectively.

Vickers hardness (WOLPERT 4325VD, WOLPERT Measuring Instruments Ltd. China) was measured under a load of 9.81 N with a dwell time of 15 s. At least 10 indentations were taken for each composition. Fracture toughness was calculated by the Anstis equation [16] as shown in Eq. (1).

$$K_{IC} = 0.016 \cdot \left(\frac{E}{H}\right)^{1/2} \cdot \left(\frac{P}{C^{3/2}}\right) \quad (1)$$

Here, K_{IC}-fracture toughness ($MPa \cdot m^{1/2}$), E-Young's modulus (GPa), H-Vickers hardness (GPa), the P-indentation load (N) and c-radial crack half-length (m).

Raman spectroscopy (HR Evolution, Horiba, Japan) was used to investigate possible structural change of the GNPs during the powder preparation and the SPS process. Morphology of the powder mixtures and microstructure of the composites were characterized by scanning electron microscopy (FESEM, JSM IT800, JEOL, Japan) and transmission electron microscopy (TEM, Talos F200x, FEI America).

Results and Discussion

Powder mixture

Raman spectroscopy of the GNPs after ultrasonic dispersion is shown Fig. 1(a). The high intensity band centered at 788 cm^{-1} and 968 cm^{-1} are exhibited, corresponding to the transverse optical (TO) and longitudinal optical (LO) mode of α-SiC, respectively [5]. In the range from 1000 cm^{-1} to 3000 cm^{-1}, the D band, G band, D' band and the 2D band linked to carbonaceous species are clearly observed. The D band at ~1350 cm^{-1} and G band at ~1580 cm^{-1} are characteristic for defects in the GNPs and the degree of crystallization in the graphite, respectively [7]. The D' band at ~1620 cm^{-1} is activated by single-phonon intervalley scattering process [17]. The 2D band near 2700 cm^{-1} is due to the doubly degenerate phonon mode belonging to the in-plane transversal optical phonon near the K points in the Brillouin zone [18]. The I_D/I_G ratio is usually used to quantify the defects of GNPs. The intensity ratio ($I_D/I_{D'}$) of D peak to D' peak is closely related to the type of graphene surface defects. When $I_D/I_{D'}$ is less than 3.5, defects associated with boundary defects in graphite, when the ratio $I_D/I_{D'}$ is less than 7, defects associated with vacancy defects in graphite [17]. The result of the intensity ratio of I_D/I_G and $I_D/I_{D'}$ are shown in the

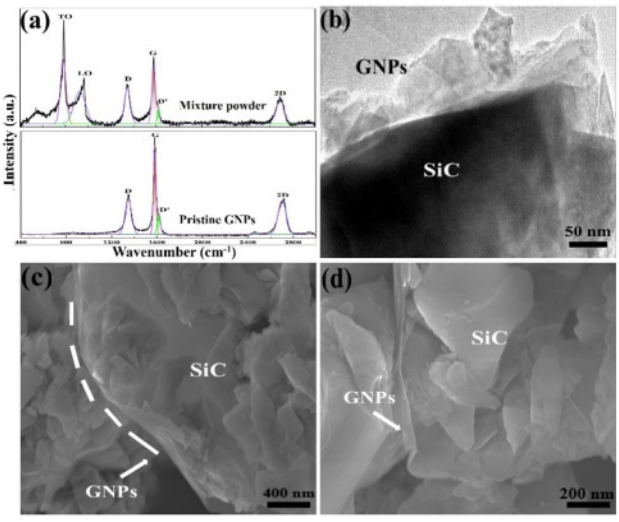

Fig. 1. A Raman spectrum (a) of the pristine GNPs and GNPs after ultrasonic dispersion; TEM (b) and SEM (c and d) of the SiC/ 2 wt.% GNPs powder mix.

Table 1. Raman band intensity ratio of pristine GNPs, mixture powder and SiC/GNPs composite.

Peak intensity ratio	Pristine GNPs	Mixture powder	SiC/GNPs composite
I_D/I_G	0.4	0.6	0.7
$I_D/I_{D'}$	1.8	2.6	4.5

Table 1. After the process of ultrasonic and magnetic stirring, the I_D/I_G and $I_D/I_{D'}$ ratios increase, indicating that the defects of GNPs increase, and a large number of boundary defects are generated [19]. As argued in Ref. [20], ultra-sonification process owns unique effects such as cavitation, cavitation bubble collapse and micro jet which could benefit dispersion of GNPs, while could also have introduced structural defects to GNPs.

TEM and SEM of the SiC/GNPs powder mixtures are shown in Fig. 1. The TEM image in Fig. 1(b) presented thin GNPs sheets with a rather large specific area. The SEM images in Fig. 1(c) and (d) showed the multilayer structures of GNPs kept among SiC particles.

Densification of the SiC/GNPs composites

In Table 2, it was showed that the density decreased when the sintering temperature was 2000°C, a slight decrease in relative density with increase of GNPs content was presented, in agreement with observations reported in documents [15]. The relative density was bellowed 98% when addition of GNPs was more than 4 wt.%. Since mechanical properties of sintered samples are sensitive with porosity, in order to eliminate the influence of porosity factors, SiC/4, 6, 8 wt.% GNPs composites were sintered at 2050°C to insure relative density of sample larger than 98%. The density of SiC composites with 4, 6, 8 wt.% GNPs is lower than that of SiC composites with 0, 1, 2 wt.% GNPs, indicating that of high content of GNPs usually inhibits sintering of SiC ceramics, resulting in some residual porosity [13]. The thermal expansion coefficient of GNPs is lower than SiC, the shrinkage of SiC ceramics is inhibited during sintering. Therefore, the density decreases with the increase of GNPs content.

The average grain size in the sintered composites is also listed in Table 2. The monolithic SiC composition without GNPs showed an average grain size ~2.5±1.1 μm. Measurements of SiC grain diameter on SEM images gave average grain sizes of the SiC/GNPs composites in range of 1.1-1.5 μm, decreasing with the GNPs content. The grain size of the 8 wt.% GNPs composition was decreased as small as 1.1±0.8 μm. SiC grain growth was hindered by presence of GNPs.

Characterization of the SiC/GNPs composites.

A value of I_D/I_G ratio of 0.7 for SiC/2 wt.% GNPs composite was calculated by the data presented in Fig. 2(a). This value was larger than that of GNPs in the mixture powder, indicating increases in defects of GNPs during SPS, damage of GNPs was unavoidable in SPS process due to high temperature and pressure [21]. According to the radio of $I_D/I_{D'}$, the disorder of GNPs gradually increased, and the structural defects showed the characteristics of vacancy defects. The vacancy defects of the GNPs in SiC/GNPs composites may be caused by atomic diffusion/surface atomic evaporation.

Fig. 2(b) shows a SEM image of polished section of the SiC/GNPs composite where 2 wt.% GNPs was added. Uniform distribution of the GNPs was illustrated. Most GNPs were exist at SiC multi-grain junctions, in consistency with López-Pernía [22]. It was clear that more homogeneous dispersion of the GNPs was needed to optimize microstructure and mechanical properties of the SiC/GNPs composites. Fig. 2(c) shows the zig-zag structure of long GNPs along the grain growth increases the contact area between GNPs and SiC grains, inhibits the SiC grains growth during the densification process.

Three different states/forms of carbon existence were revealed in the SiC/GNPs composites. The first state was soft carbon presented at SiC boundaries, as illustrated

Table 2. SPS condition, bulk density, relative density, and grain size measurement for/of the SiC/GNPs composites.

Experimental materials	Temperature (°C)	Bulk density ($g \cdot cm^{-3}$)	Relative density (%)	Grain size (μm)
SiC+0 wt.% GNPs	2000	3.17	99.0	2.5±1.1
SiC+1 wt.% GNPs	2000	3.15	98.7	1.5±0.9
SiC+2 wt.% GNPs	2000	3.14	98.9	1.3±0.7
SiC+4 wt.% GNPs	2000	3.08	97.8	–
SiC+6 wt.% GNPs	2000	3.00	96.8	–
SiC+4 wt.% GNPs	2050	3.12	98.9	1.3±0.7
SiC+6 wt.% GNPs	2050	3.09	98.7	1.2±0.7
SiC+8 wt.% GNPs	2050	3.05	98.3	1.1±0.8

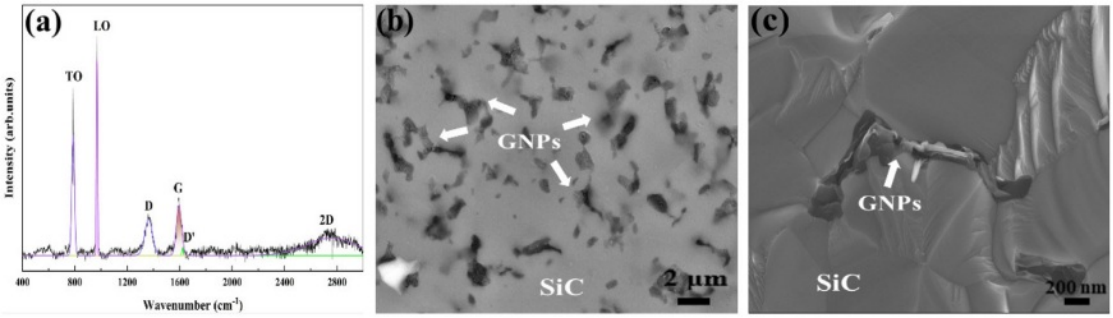

Fig. 2. A Raman spectrum (a), HRSEM (b) and SEM fractured surface image (c) of the SiC/2 wt.% GNPs composite prepared by SPS.

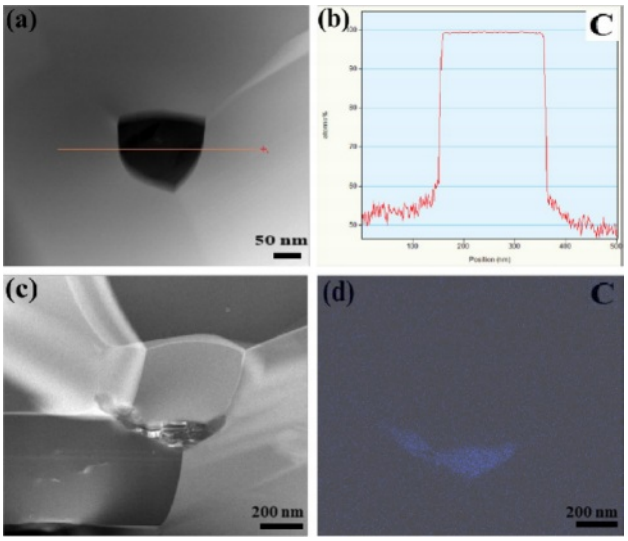

Fig. 3. STEM-HAADF (a, c), EDS line scan (b), and EDS elemental mapping (d) of the SiC/2 wt.% GNPs sample.

by Fig. 3(a) and 3(b). These soft carbon regions could be formed from carbonized glucose. Fig. 3(c) and 3(d) illustrated the second form of the carbon existence, i.e., GNPs thick layers extending along the SiC grain boundaries and having wrinkled morphology. Fig. 3(c) also shows that there is no amorphous or second phase material produced between SiC/GNPs, indicating that the interface bonding of SiC/GNPs is physical bonding. There are wrinkles and ups and downs on the surface of graphene. This rough surface is conducive to the formation of mechanical locking between graphene and matrix materials. This strong interfacial bonding could help improve mechanical properties (such as strength and fracture toughness) of the materials.

The third state of carbon existence was thin graphene sheets that were consisted of only a limited number of graphene layers as evidenced by TEM, HRTEM and EDS line scan in Fig. 4. In Fig. 4(a), the SiC-SiC boundary showed a dark contrast in comparison with the neighboring SiC grains, indicating phase of lower average atomic order relative to SiC existed there. Therefore, EDS line scans were carried out across such SiC-SiC boundaries. Figs. 4(b) and (c) are results of the EDS scan along the line marked in Fig. 4(a). The changes in the C and Si signal intensities evidenced existence of a layer of carbon along the interface, and the thickness of the C-layers was well below the conventional TEM observation. Figs. 4(d) and (e) are HRTEM and IFFT image of a SiC-SiC boundary showing the same relatively dark contrast. The fringes measured a face spacing of 0.324 nm, in consistency with multi-layered graphene

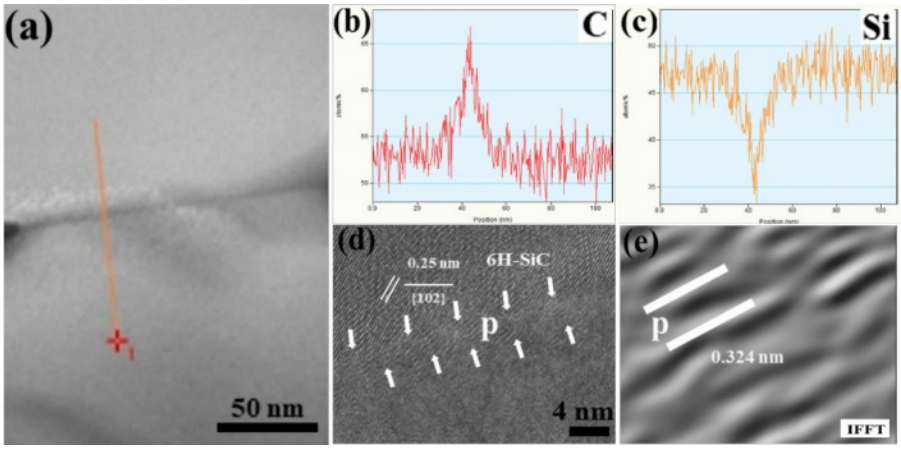

Fig. 4. TEM-BF (a), EDS scans (b, c) along the line in figure (a), and HRTEM (d) of a SiC-SiC interface in the SiC/2 wt.% GNPs sample, IFFT image taken from P point (e), showing a thin GNP sheet consisted of (6-10) C-layers existing along the grain boundary.

(0.335 nm) [23]. The EDS and HRTEM results indicated that GNPs may exist as very thin layer graphene (single layer or 6-10 layers) in the composites and these thinner layer graphene distribute between SiC grain boundary. In the graphene, the distorted atomic planes can have various causes, such as its synthesized process, applied pressure over the SPS process, etc.

In summary, carbon is present in three states/forms, i.e., soft carbon phase, thick-layered graphene, and thin-layered graphene. It was worth noticing that only the thin-layered graphene could extend along the SiC grain boundaries extensively and thus closely wrapped the SiC grains. It was also clear that, the desired state of GNPs existence should be such thin-layered graphene, and content of which was closely dependent on dispersion of the GNPs raw material in the SiC/GNPs mix before SPS. In terms of the dispersion of GNPs, although ball-milling plus ultrasonication was commonly thought as useful, a completely dispersion of graphene sheets is still a challenge in processing of ceramic composites containing GNPs.

Mechanical properties

Mechanical properties of the composites are shown in Fig. 5. Vickers hardness of the SiC ceramic without GNPs addition was 23 GPa. It was increased up to 25 GPa when 1 wt.% or 2 wt.% GNPs was added. SEM image (Fig. 2b) shows that the GNPs was uniformly dispersed in SiC/1, 2 wt.% GNPs composites. And TEM image (Fig. 4d) shows that there is a thin layer of GNPs. The thin layer of GNPs has good deformability and play a role in preventing the decrease of Vickers indenter, so the hardness increased. Extension of the thin-layered GNPs across SiC grain boundaries was believed to be the reason for the increased hardness for ultra-high elastic modulus of thin GNPs. Here, the ~7% increase in Vickers hardness was by no means not insignificant in view of the very limited content of the desired thin-layered graphene in the 1 wt.% or 2 wt.% compositions. In addition, the refined microstructure of SiC ceramics with additions of GNPs also help increase hardness to some extent [12, 24]. With more GNPs addition, however, Vickers hardness gradually decreased and the hardness of the 8 wt.% GNPs composition was only 21 GPa. The SiC/GNPs composites under investigation were in fact almost fully dense (>98%), to exclude effect of residual porosity on hardness of the materials. With the increase of GNPs content, the GNPs agglomerates in SiC/GNPs composites, and the weak van der Waals force between the GNPs layers induces the decrease of Vickers hardness [15].

In Fig. 5(a), the effect of GNPs on fracture toughness of the SiC/GNPs composites is illustrated. The monolithic SiC ceramic without GNPs addition had a fracture toughness of 3.1 MPa·m$^{1/2}$; It was decreased slightly in the 1 wt.% and 2 wt.% GNPs composition (~3.0 MPa·mm$^{1/2}$), followed by a steady increase in fracture toughness when more GNPs was added. For detail, the fracture toughness of the 8 wt.% GNPs composition reached ~3.8 MPa·mm$^{1/2}$, a value 23% larger than that of the monolithic SiC ceramic.

Fracture surfaces of the 2 wt.% and 4 wt.% compositions are showed in Fig. 5(b) and (c). Uniform dispersion of GNPs in the SiC matrix was demonstrated. However, GNPs agglomeration became obvious at higher GNPs contents. The fracture surfaces were dominated by trans-granular fracture, with pull-out of GNPs sheet commonly observed. Fig. 5(d) depicted pull-out of the graphene sheets at higher magnifications. Pull-out of the graphene sheets indicated consummation of fracture energy during crack propagation, an effective toughening mechanism for ceramic material [25-27].

GNPs wrapping SiC grains was also illustrated in Fig. 5(d) and (e). Distribution of GNPs along SiC grain

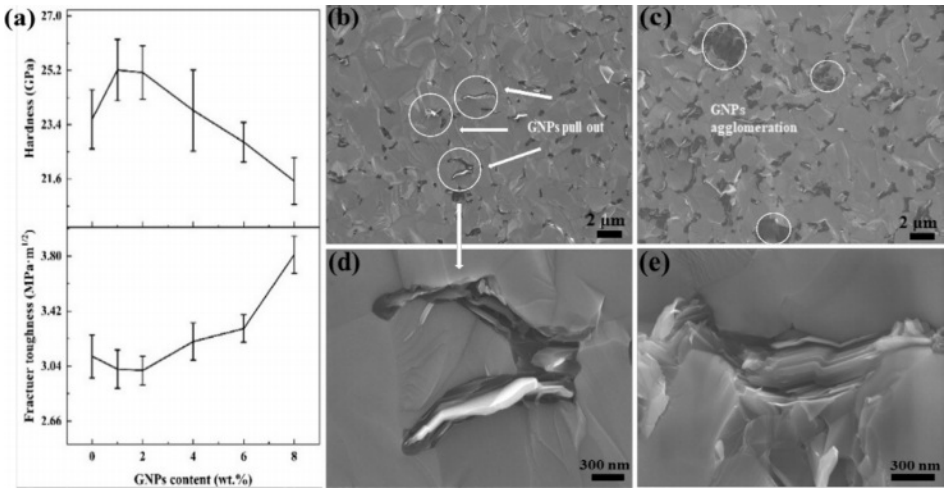

Fig. 5. (a) Vickers hardness and fracture toughness of SiC/GNPs composite, (b) fracture surface of SiC/2 wt.% GNPs composite, (c) fracture surface of SiC/4 wt.% GNPs composite, (d) the enlarged view of the (b) circle area, (e) relative sliding, or delamination between graphene layers on the fractured surface.

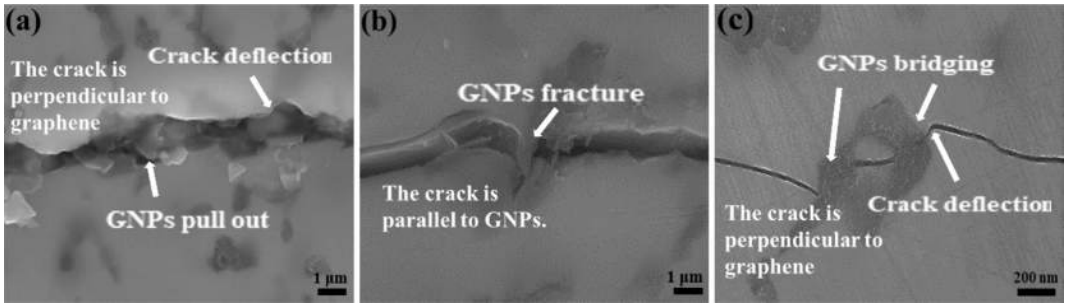

Fig. 6. Crack propagation at Vickers indent corners showing GNPs pull-out (a), delamination (b) and crack deflection/bridging (c) as main toughening mechanism.

boundaries were thought to mitigate strain mismatch between adjacent grains, reducing microcracking due to the lowered strain energy [28]. Fig. 5(e) also showed sliding and delamination of the GNPs sheets, a situation similar with graphite. Because of high strength and elastic modulus within the C sheets while weak bonding by Van der Waals force between the C-sheets, the thick-layered GNPs tend to delaminate and slide along the C-sheets to dissipate fracture energy, with the increase of GNPs content, the number of pull-out and sliding of graphene increases, hence higher fracture toughness [12, 29].

Crack propagation behavior at Vickers hardness indent corners was investigated to further demonstrate toughening mechanisms of the GNPs additions. As shown in Fig. 6, bridging, pull-out of GNPs sheets and crack deflection were common. Delamination of GNPs was presented in Fig. 6(b) while crack bridging by GNPs ligament was presented in Fig. 6(c). Fig. 6(a-c) also shows that when the crack meets transverse GNPs, the crack diffuses in the horizontal direction and the three-dimensional direction of the longitudinal GNPs, and the GNPs is detached/pulled out. Due to the increase of the crack diffusion path, the crack stress concentration is effectively reduced, thereby toughening the ceramic material.

When the crack encounters vertically distributed graphene at the end of the crack in the process of crack propagation, the crack deflection is mainly caused by graphene breakage or graphene monolayer slip or breakage, which increases the total fracture surface area and achieves the purpose of toughening.

Before going to conclusion, here gave a very brief discussion to argue for the effects of GNPs addition on mechanical properties of the SiC/GNPs composites. It is clear that sufficient dispersion of graphene sheets is still a big challenge for processing ceramic composites containing GNPs. Insufficient dispersion could be the reason for coexistence of three states/forms of C, including soft C, thick-layered graphene (several hundreds of layers of C-sheets) and thin-layered graphene (less than a few tens of layers of C-sheets) in the SiC/GNPs composites.

It is also clear that the significant increase in Vickers hardness observed in the 1 and 2 wt% GNPs compositions relative to monolithic SiC ceramics was attributed to the thin-layered graphene sheets in the composites. However, the other two states/forms of GNPs may serve better in toughening the SiC/GNPs composites.

Due to the lubricant feature of soft carbon, the soft carbon phase present in the SiC/GNPs composites may help slide of SiC grains against each other, leading to a softening effect of the structure and promoting deformation under the Vickers tip indentation [30]. The second state/form of the thick-layered graphene extending along the grain boundaries inhibited growth of the SiC grains. The microstructure refinement effect of the GNPs additions was clearly showed in Table 2 by the grain size measurements, and the finer microstructure might increase the hardness by hindering dislocation mobility [24]. However, when the graphene additions were larger than 4%, most of the graphene existed as carbon agglomerates (Fig. 5c). In this case, the low strength of the carbon agglomerates would play a negative role in reinforcing the composites due to weak van der Waals forces between the C-atom layers, causing decrease in hardness as GNPs content increased.

Graphene has good deformability on scale of C-atomic single plane. Therefore, the thin-layered graphene distributed along the grain boundaries are crucial to reinforcing of the composite materials. In this work, Vickers hardness was increased by 7% when 1 wt.%, 2 wt.% GNPs was added. Although content of monolayer or thin-layered graphene in the composites are much less than 1%, the thin-layered graphene existing along the SiC boundaries contributed significantly to the mechanical properties of the composites. In documents [10, 11], 162% and 55% increase in fracture toughness and strength should be results of homogeneous dispersion of such thin-layered graphene sheets.

Increase in fracture toughness by the different contents of GNPs additions was attributed to pull-out, crack deflection and bridging of the GNPs sheet. In case of transgranular fracture (Figs. 5b and 5c), the crack extends when stress level at the crack tip reaches theoretical strength of SiC. Presence of GNPs along the grain boundaries lowers fracture energy required for crack propagation, to facilitate crack deflection and

bridging. On the other hand, when stress is transmitted through graphene, the stress field is located at the front while the graphene is at the crack wake. The graphene sheets bridging the crack wake surely increase fracture toughness.

Conclusions

SiC/GNPs composites with additions of 0-8 wt.% GNPs were prepared by SPS at 2000-2050°C. The relative densities >98% were reached despite the different GNPs contents. Raman spectra showed a significant increase in defect concentration in GNPs due to high temperature and pressure used in SPS. SEM showed uniform dispersion of the graphene in the microstructures. The zig-zag structure of GNPs along the grain growth increases the contact area between GNPs and SiC grains, inhibits the SiC grains growth during the densification process. TEM showed that the GNPs and SiC interfaces were mechanically interlocked. Vickers hardness of SiC/GNPs with 1 and 2 wt.% GNPs additions were increased by 7% relative to monolithic SiC due to thin-layered graphene extend along the SiC grain boundaries and thus closely wrapped the SiC grains. Fracture toughness of the compositions were increased as GNPs addition increase although slightly decreased as 1% and 2% GNPs addition. GNPs pull-out, delamination, crack bridging and deflection were recognized as the main toughening mechanisms in the SiC/GNPs composites.

Acknowledgements

This work was supported by the Key R&D projects of Ningxia Autonomous Region [2021BFH03003] and National Natural Science Foundation of China [No. 52162008].

References

1. S. Li, X.D. Luo, C.C. Wei, P.L. Gao, P. Wang, and L.J. Zhou, J. Alloys. Compd. 834 (2020) 155252.
2. D. Sciti and A. Bellosi, J. Mater. Sci. 35[15] (2000) 3849-3855.
3. Y. Cao, R.Y. Deng, J.L. Hu, J.X. He, D.P. Lei, Z.J. Chen, and Y.X. Peng, J. Ceram. Process. Res. 24[2] (2023) 321-328.
4. C.G. Lee, X.D. Wei, J.W. Kysar, and J. Hone, Sci. 321[5887] (2008) 385-388.
5. A. Nieto, A. Bisht, D. Lahiri, C. Zhang, and A. Agarwal, Int. Mater. Rev. 62[5] (2016) 241-302.
6. I.-J. Shon, Ceram. Process. Res. 17[11] (2016) 1171-1174.
7. C. Chen, X.C. Han, H.H. Shen, Y.Q. Tan, H.B. Zhang, Y. Qin, and S.M. Peng, Ceram. Int. 46[14] (2020) 23173-23179.
8. M. Nader, F. Aldinger, and M. Hoffmann, J. Mater. Sci. 34[6] (1999) 1197-1204.
9. T. Maruyama, Y. Yamashita, T. Saida, S.-I. Tanaka, and S. Naritsuka, J. Cryst. Growth. 468 (2017) 175-178.
10. A.N. Manuel Belmonte, Pierre Boutbien, Benito Román-Manso, María I. Osendi, Pilar Miranzo, Scripta. Mater. 113 (2016) 127-130.
11. P. Miranzo, C. Ramírez, B. Román-Manso, L. Garzón, H. Gutiérrez, M. Terrones, C. Ocal, M.I. Osendi, and M. Belmonte, J. Eur. Ceram. Soc. 33[10] (2013) 1665-1674.
12. Q.S. Li, Y.J. Zhang, H.Y Gong, H.B. Sun, W.J. Li, L. Ma, and Y.S. Zhang, J. Mater. Sci. Technol. 32[7] (2016) 633-638.
13. E. Bódis, I. Cora, C. Balázsi, P. Németh, Z. Károly, S. Klébert, P. Fazekas, A.M. Keszler, and J. Szépvölgyi, Ceram. Int. 43[12] (2017) 9005-9011.
14. J.M. Anna Kaźmierczak-Bałata, Ceram. Int. 44[9] (2018) 10273-10280.
15. X.Z. Guo, R. Wang, P. Zheng, Z.J. Lu, and H. Yang, Adv. Appl. Ceram. 118[7] (2019) 409-417.
16. R. Sedlák, A. Kovalíková, V. Girman, E. Múdra, P. Rutkowski, A. Dubiel, and J. Dusza, J. Eur. Ceram. Soc. 37[14] (2017) 4307-4314.
17. N. Lu, J.X. Liu, G. He, and J.T. Li, Solid. State. Phenom. 281 (2018) 125-130.
18. A. Eckmann, A. Felten, A. Mishchenko, L. Britnell, R. Krupke, K.S. Novoselov, and C. Casiraghi, Nano. Lett. 12[8] (2012) 3925-3930.
19. J.Z Zhun, Y.M. Shang, and Y. Liu, Petrochemical. Technology. 51[11] (2022) 1323-1329.
20. B. Zhang, T.J. Chen, L.Y. Wang, and B.Q. Yang, J. Funct. Mater. 50[08] (2019) 8133-8139.
21. V.-H. Nguyen, S.A. Delbari, M. Shahedi Asl, Q.V. Le, A. Sabahi Namini, Z. Ahmadi, M. Farvizi, M. Mohammadi, and M. Shokouhimehr, Ceram. Int. 47[9] (2021) 12459-12466.
22. C. López-Pernía, Á. Gallardo-López, A. Morales-Rodríguez, and R. Poyato, J. Eur. Ceram. Soc. 39[14] (2019) 4435-4439.
23. L.X. Liu, Y. Wang, X.H. Li, L. Xu, X.X. Cao, Y.H. Wang, Z.G. Wang, C.M. Meng, W.J. Zhu, and X.P Ouyang, J. Am. Ceram. Soc. 99[1] (2016) 257-264.
24. M. Balog, J. Kečkéš, T. Schöberl, D. Galusek, F. Hofer, J. Křesťan, Z. Lenčéš, J.-L. Huang, and P. Šajgalík, J. Eur. Ceram. Soc. 27[5] (2007) 2145-2152.
25. C. Yun, Y. Feng, T. Qiu, J. Yang, X. Li, and L. Yu, Ceram. Int. 41[7] (2015) 8643-8649.
26. Y.H. Huang, D.L. Jiang, X.F. Zhang, Z.K. Liao, and Z.R. Huang, J. Eur. Ceram. Soc. 38[13] (2018) 4329-4337.
27. Z.Y.B. Zeng, Y.Z. Liu, W.P. Chen, X.Q. Li, Q.F. Zheng, K.L. Li, and R.R. Guo, J. Am. Ceram. Soc. 101[8] (2018) 3498-3507.
28. J.H. Gong, J. Adv. Ceram. 42 (2021) 287-428.
29. A. Nieto, D. Lahiri, and A. Agarwal, Mat. Sci. Eng. A-Struct. 582 (2013) 338-346.
30. B. Lanfant, Y. Leconte, G. Bonnefont, V. Garnier, Y. Jorand, S. Le Gallet, M. Pinault, N. Herlin-Boime, F. Bernard, and G. Fantozzi, J. Eur. Ceram. Soc. 35[13] (2015) 3369-3379.